Signatures of fatigue crack growth from acoustic emission repeaters

Théotime de la Selle, Julien Réthoré, Jérôme Weiss, Joël Lachambre, Stéphanie Deschanel

Engineering Fracture Mechanics 309 (2024) 110388

Contents lists available at ScienceDirect

Engineering Fracture Mechanics

journal homepage: www.elsevier.com/locate/engfracmech

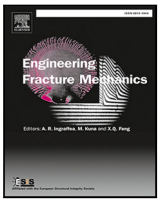

Signatures of fatigue crack growth from acoustic emission repeaters

Théotime de la Selle [a,*], Julien Réthoré [c], Jérôme Weiss [b], Joël Lachambre [a], Stéphanie Deschanel [a]

[a] Univ Lyon, INSA Lyon, Université Claude Bernard Lyon 1, CNRS, MATEIS, UMR5510, Villeurbanne, 69621, France
[b] ISTerre, CNRS and Université Grenoble-Alpes, CS 40700, Grenoble, 38053, France
[c] Nantes Université, Ecole Centrale Nantes, CNRS, GeM, UMR 6183, 1 rue de la Noë, Nantes, F-44321, France

ARTICLE INFO

Keywords:
Fatigue crack growth
Acoustic emission
Multiplets
Digital image correlation
Crack tip plasticity
Crack rubbing

ABSTRACT

Since the discovery of fatigue phenomena, scientific research has constantly sought to understand and anticipate the failure of materials due to fatigue to mitigate unforeseen accidents and malfunctions in various technical fields. Numerous studies using acoustic emission (AE) – a key method in non-destructive testing – have shown a correlation between acoustic activity and fatigue damage. However, these measurements suffer from the non-specific nature of AE signals, which may be due to various physical sources. To investigate further the mechanisms of AE emission associated with fatigue, we study the groups of acoustic signals generated by fatigue cracking in metals. These so-called *acoustic multiplets* are characterized by highly correlated waveforms, are repeatedly triggered over many successive loading cycles at nearby stress levels and originate from a single location. These acoustic signatures produced during the propagation of fatigue cracks in alloys are automatically detected by a dedicated algorithm, grouped into multiplets and analyzed to understand the physical mechanisms from which they originate. By synchronizing their detection with digital image correlation measurements of fracture mechanics quantities, the investigation of this acoustic emission phenomenon shows that two mechanisms are at the origin of the multiplets: repeated local friction over fracture surfaces, and incremental crack propagation in the Paris regime, probably due to the reactivation of crack tip plasticity at each cycle. These two multiplet types serve as acoustic signatures, distinctly indicating the existence and propagation of a fatigue crack.

1. Introduction

1.1. Context: fatigue of materials

Since the historical catastrophic accidents in the naval, railway and aeronautical industries in the middle of the 20th century [1], fatigue failure and the associated crack propagation became a subject of upmost importance in fracture mechanics. Fatigue failure occurs when parts and structures are subjected to cyclic mechanical or thermo-mechanical stress during several hundreds to thousands of loading cycles, even at stress levels far below the yield stress. The fatigue failure issue is reinforced by the fact that the initiation and slow propagation of fatigue cracks in a system are hardly detectable in-operando, as they do not induce

* Corresponding author.
E-mail address: Theotime.de-la-selle@insa-lyon.fr (T. de la Selle).

https://doi.org/10.1016/j.engfracmech.2024.110388
Received 7 March 2024; Received in revised form 16 July 2024; Accepted 8 August 2024
Available online 14 August 2024

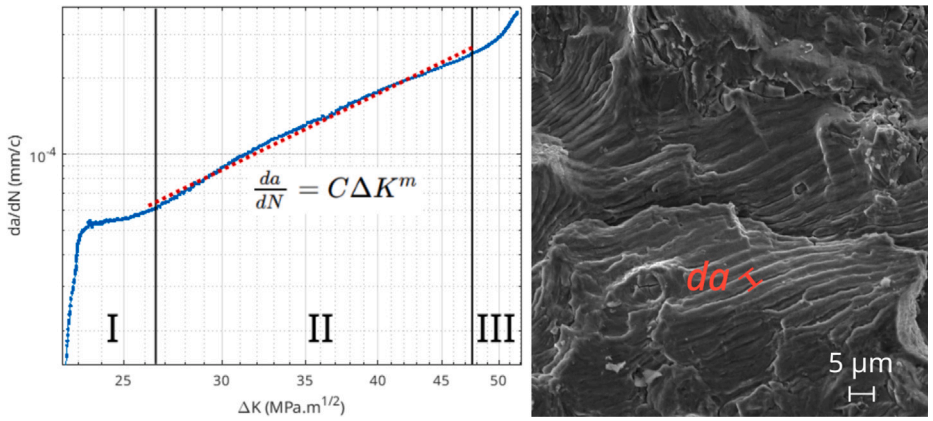

Fig. 1. Left: crack growth rate da/dN versus the stress intensity factor range ΔK for a load-imposed ($R = 0.1$) fatigue test on a 5083 Aluminium alloy sample, showing the three fatigue regimes and the crack propagation Paris' law, $da/dN = C\Delta K^m$(regime II) with $m = 2.4$ and $C = 2.1 \cdot 10^{-8}$. **Right** : Scanning Electron Microscopy (SEM) post-mortem image of fatigue striations on a fracture surface in a 5083 aluminium alloy sample after a fatigue test.

significant changes of the physical or mechanical properties of the entire structure until approaching final failure. As a result, *early*, non-destructive detection of fatigue crack propagation is still a major challenge.

The mechanisms of fatigue crack initiation and propagation are now well identified [2,3] in metallic materials, particularly for low-cycle fatigue (LCF) in which plastic yield is crossed at each cycle. Under these conditions, localized plastic deformation occurs via persistent slip bands (PSB) [4], leading to stress concentrations and the initiation of micro-cracks. Three stages of crack propagation are generally considered. Stage I, i.e. the onset of propagation limited to a few grain sizes, is classically associated with crystallographic rupture since the number of active slip systems is low at the crack tip. Stage II, called the Paris' regime [5], is the longest stage in most cases as it can last several thousands of cycles, representing a significant fraction of the total lifetime. In this regime, the crack propagates slowly by successive increments of the order of a few micrometers at each cycle along a plane perpendicular to the largest principal tensile stress. This stage is often called the *stable crack growth* phase, which can be identified from post-mortem examinations of fracture surfaces through clearly visible striations (an example for a 5083 aluminium alloy is shown on Fig. 1, on the right). Then, during stage III, crack propagation accelerates sharply, rapidly leading to macroscopic rupture, which we seek to avoid through preventive measures. These three stages are illustrated in Fig. 1 where the crack growth rate da/dN is plotted as a function of the stress intensity factor range ΔK, over a loading cycle, for a fatigue test performed on a 5083 aluminium alloy. A key safety issue is therefore to be able to detect in-operando (i.e. non destructively) the presence of a running fatigue crack within a part/structure well before the onset of stage III, i.e. during the Paris' regime.

1.2. Acoustic emission in fatigue

Acoustic emission (AE) is a non-destructive technique (NDT) based on the passive recording of dynamic surface motions (elastic waves) caused by spontaneous, sudden releases of elastically stored energy. It has long been proposed as a monitoring fatigue tool [6]. The physical sources of AE in metals can be dislocation motions [7,8], phase transformations [9,10], or microcracking [11]. Two types of AE can be recorded: discrete and continuous [12]. The *discrete* AE is made of well defined transient bursts (timescale of µs to ms) above a background, while the *continuous* emission consists of a slow (compared to the timescale of AE bursts) evolution of the background as the result of the cumulative effect of numerous, small and uncorrelated (in space and time) sources that cannot be individualized by the recording system [8]. In our study, we analyze only the burst-type waveforms (example of AE waveform (WF) in Fig. 2), recorded when the signal crosses a threshold set by the user, above the background (dashed black horizontal lines).

Most previous works on AE during fatigue crack growth (FCG) have focused on the overall AE activity, considering e.g. the evolution of the count rate, or the number of bursts (called *hits* in AE studies) detected per cycle [13,14]. Actually, stage II is known to be relatively silent compared to stages I and III. Furthermore, the AE activity during stage I is primarily associated with plasticity, not crack initiation or propagation. Thus, such evolution or correlations between these global variables and the crack growth rate da/dN only become significant close to final failure, during stage III, or depend strongly on loading conditions and specimen properties [15].

Thus, the evolution or correlations between these global variables and the crack growth rate da/dN only become significant close to final fracture, during stage III, or depend strongly on loading conditions and sample properties.

Therefore, the detection of fatigue crack growth from these global AE methods suffers from limitations: tracking slow FCG during the Paris' regime by a global measure is extremely difficult due to, notably, a high sensitivity to signal-to-noise ratio (SNR). Besides this, the non-specific nature of AE signals, which can be generated by all physical sources presented above, or environmental noise, requires additional classification efforts. Thus, several studies have attempted to identify acoustic fatigue crack signatures through, for example, sophisticated time and frequency domain features of AE signals [16] or waveforms information (Shannon) entropy [17].

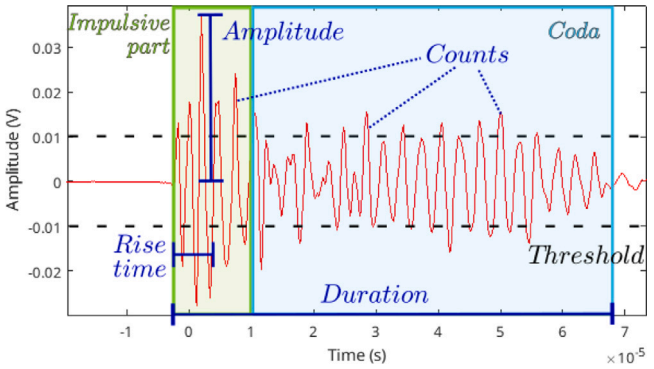

Fig. 2. A typical AE burst-type waveform and some classical description features extracted from it.

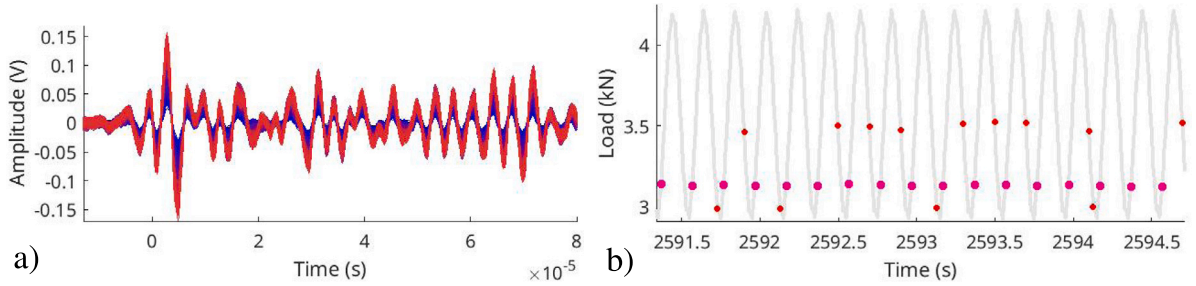

Fig. 3. **(a)** 3760 superposed waveforms belonging to the multiplet presented in **(b)**. Coloration from blue to red shows the increasing time of arrival. **(b)** Example of multiplet occurrence during a load-imposed ($R = 0.1$) fatigue test on a 5083 aluminium alloy. The fatigue cycles are represented by the gray solid line, large magenta dots correspond to AE signals belonging to a multiplet, and small red ones to other recorded signals.

Because of the high variability of AE waveforms due to sensor response, material properties, mechanical behavior of the propagation medium affected by strain-hardening and damage, such sophisticated features are difficult to generalize and are sensitive to SNR. Similarly, elaborate methods have been proposed to discriminate the AE signatures of different source mechanisms based on classical features of the AE signals. For example, the k-means clustering algorithm has been used to group different source mechanisms [10].

1.3. Acoustic multiplet : signature of a unique source

A recent project [18,19], conducted by two co-authors of this paper, highlighted, for the first time, very specific AE signals, characterized by almost identical waveforms (Fig. 3a), triggered at each fatigue cycle at an almost unchanged load level (Fig. 3b), over a very large number of successive cycles (from tens to several hundreds). These signals are defined as a specific signature of a single source associated with fatigue cracking under the Paris regime (stage II) and are called *acoustic multiplets* in reference to an analogous phenomenon in seismology [20]. Although, they differ from seismic *multiplets* or *repeaters*, for which the repeatability mechanism is not related to cyclic loading but to a stick–slip mechanism under a slow far-field driving and which are not as periodic as in the fatigue context. In context of fatigue damage, AE multiplets have two major advantages: they enable early in-service detection of a crack while mitigating SNR problems [21], and offer a new way of studying crack growth mechanisms.

Although we have previously demonstrated the correlation between these AE multiplets and fatigue cracking [18], their source mechanisms remain to be clarified. Indeed, in this former study, only macroscopic stress and strain, as well as AE, were recorded. In addition, due to the cylindrical specimen geometry, several cracks may have propagated simultaneously. Hypotheses on the source mechanisms of multiplets were formulated: multiplets emitted during the loading phase of the fatigue cycle ($d\sigma/dt > 0$) may be associated to incremental fatigue crack propagation, while those emitted during unloading may be associated with rubbing on the crack faces.

The aim of the present paper is to explore these hypotheses and determine the source mechanisms of AE multiplets in fatigue from a simultaneous analysis of AE, as well as stress and strain fields around the crack tip, from digital image correlation on notched specimens.

2. Methods

To link fatigue crack growth to multiplets, we have implement an AE multiplets detection coupled to a crack tip detection and crack stress state estimation from digital image correlation (DIC). This requires a rigorous synchronization of AE and image

Table 1
Average mechanical properties of 5083 in normalized condition.

Re	*Rm*	*E*	*ρ*	*ν*	*HB*
126 MPa	262 MPa	70 GPa	2700 kg/m^3	0.33	75 HB

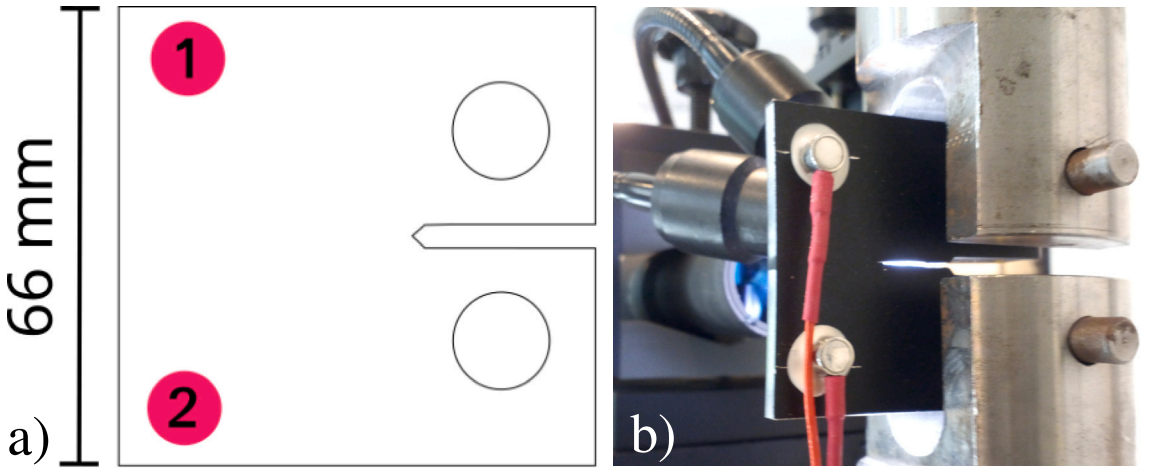

Fig. 4. **(a)** Compact tension (CT) specimen geometry and sensors positions (red numbered circles). **(b)** Fatigue test setup showing a CT specimen mounted in grips with 2 nano 30 sensors coupled to the surface and the camera behind.

recording. In the following sections, we present the experimental methods, AE recording, image acquisition, and their respective analyses to detect multiplets and determine crack tip positions, stress intensity factors (SIF) and crack opening displacements (COD) from displacement fields around the crack.

2.1. Material and mechanical testing

FCG experiments are performed on compact tension (CT) specimens (see geometry in Fig. 4**a**) made of 5083 aluminium alloy (see mechanical properties in Table 1) monitored by AE and DIC (details given below). The initially notched, but non-cracked, specimens were tested under load-imposed (constant ΔP) cyclic loading at 5 Hz until final rupture.

Two different load ratios $R = R_P = \frac{P_{min}}{P_{max}} = 0.1$ or 0.7 were applied to analyze the effect of crack closure on crack propagation and AE multiplets emission. Since a high R (e.g. $R = 0.7$) is a condition classically used to prevent crack closure, a strong reduction in the crack faces rubbing could be expected in this case. The multiplets resulting from this rubbing mechanism can therefore be studied by a comparison with the case $R = 0.1$.

Mechanical noise generated by the hydraulic system of the fatigue machine can be recorded by the sensors within their frequency bandwidth. We have therefore inserted teflon rings between the CT specimen holes and the pins to filter out this noise. Fig. 4**b** shows the fatigue setup. Note that $R = 0.1$ and $R = 0.7$ experiments have almost the same maximum load P_{max}, to avoid damage of the teflon rings. Thus ΔP at $R = 0.7$ is far smaller than ΔP at $R = 0.1$. As a result, there is a significant difference, in terms of crack propagation rate, between the experiments at $R = 0.1$ (significantly faster) and those at $R = 0.7$.

2.2. Acoustic emission : recording, multiplets classification and analysis

2.2.1. Acoustic emission setup

For each test, we fixed two Physical Acoustic Corporation sensors to the sample surface (not necessarily the same, see Table 2 ; their respective positions is represented in Fig. 4**a**). During these tests, waveforms detected above a threshold are sampled at 5 MHz. The AE triggering threshold (see 1.2) is defined based on a preliminary cyclic load-imposed loading below the material's yield stress for a few minutes. Given that no AE bursts are triggered in this condition, the threshold is selected just above the ambient noise (coming from fatigue machines and assembly mounting) recorded by the AE system. The acquisition threshold in our tests was set within the range [35–40] dB (depending on maximum load level and teflon ring damage), for a classical hydraulic fatigue machine. Note that in the AE dataset, we also register the measured load to precisely synchronized AE and image acquisitions (see Section 2.4).

Table 2
Sensors references (PAC), respective operating frequency ranges (kHz) and resonant frequencies (kHz).

Sensor reference	Micro200	Micro80	Nano30
Frequency range	[500, 4500]	[200, 900]	[125, 750]
Resonant frequency	(*wideband*)	300	200

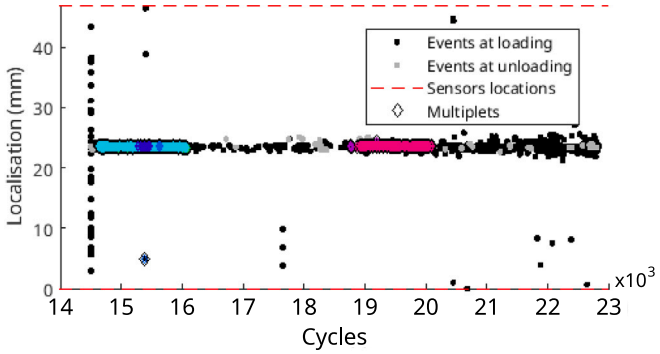

Fig. 5. 1D localization of AE signals versus number of cycles during a load-imposed ($R = 0.1$) fatigue test performed on a 5083 aluminium alloy. Detected multiplets are represented by colored diamonds. Due to a test pause for camera displacement on crack tip, the loading begins at 14 500 cycles.

2.2.2. Multiplets detection

We have presented in another paper a method based on a density-based data clustering algorithm (DBSCAN) and a dissimilarity metric derived from the cross-correlation of AE waveforms to detect and classify AE multiplets in the case of fatigue [21]. These automated algorithms can be used for both laboratory testing and industrial fatigue cases, and are designed to operate in-operando. They are essentially based on the level of similarity (measured from cross-correlation) between AE waveforms: waveforms belonging to the same multiplet are strongly similar (see Fig. 3**a**). We use this method here to detect and classify AE multiplets (AE repeaters) during our laboratory fatigue tests.

2.2.3. Multiplets analysis

To ensure that multiplets signals are due to the presence of a crack, we compute a 1D location of signals sources: when the two sensors record a burst originating from the same mechanical wave emitted by a single AE source, a 1D spatial location of this source can be calculated. A triangulation based on the known wave speed in the material and the difference $\Delta t = t_1 - t_2$ of arrival times t_1 and t_2 defined by first threshold crossings respectively on sensors I and II (see [18] for more details) provides a measure of the source position projected on the axis passing by the two sensor positions. As the sensors are located on either side of the crack path, we can check that the sources of the multiplets are located along this path, as shown in Fig. 5 (multiplets are colored marks).

2.3. Physical crack properties from digital image correlation analysis

2.3.1. Digital image correlation setup

Each CT specimen is covered by a black and white speckle, necessary for proper operation of the DIC method. A black uniform surface is first sprayed onto the surfaces, then airbrushed in two passes, white paint followed by black, to apply fine speckles of about a few tens of microns. The resulting speckles can be seen in Fig. 6. We use an OPTRONIS camera, model CP70-12-M-188 with a x2 magnification telecentric lens, to capture images in a region of interest (ROI) of a few millimeters centered around the crack tip. One pixel on the sensor represents 2.75 µm on the specimen.

To accurately correlate the stress state around the crack with acoustic emissions, numerous images need to be captured at each cycle to describe the entire load cycle. To this end, an homemade device records the measured load of the fatigue machine and triggers the camera at a constant frequency of 30 frames/cycle.

2.3.2. Displacement fields

The images are post-processed by digital image correlation, which involves solving the optical flow equation (Eq. (1)), assuming that, for all points $\underline{x}$, the variation in gray levels between f and g (gray levels in the reference and deformed states, respectively) are only due to $\underline{u}(\underline{x})$, the displacement of the material points.

$$f(\underline{x}) = g(\underline{x} + \underline{u}(\underline{x})) \tag{1}$$

A global finite element DIC method [22] is used to determine the displacement field $\underline{u}(\underline{x})$ of each deformed image compared to the reference image, which is recorded at minimum load before starting cycling loading. To resolve the optical flow equation, a non-linear least-squares resolution method (minimization of residuals by solving a series of linear systems until convergence is reached)

Table 3
DIC parameters.

Software	UFreckles (Réthoré, 2018[23])
Method	Global finite element
Element	13.75 µm (square-shaped 4-node)
Post-filtering	None

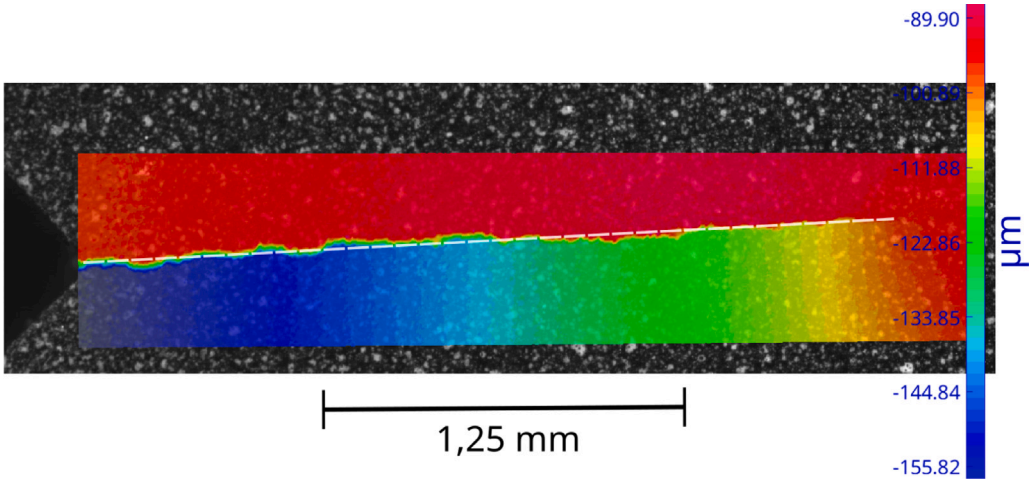

Fig. 6. Displacement field $\underline{u}_y(\underline{x})$ obtained by DIC performed on an image captured during a load-imposed FCG test at $R = 0.1$ on a 5083 aluminium alloy CT specimen around the cycle $47 \cdot 10^3$ (reference image taken at minimum load, before cycling began). The dashed white line symbolizes the mean crack path.

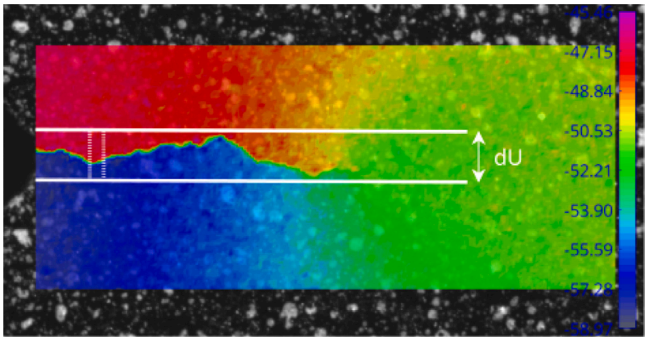

Fig. 7. Computation of the displacement difference dU_y between 2 horizontal lines above and below the crack path from displacement field on an image captured at maximum load during a load-imposed FCG test at $R = 0.7$ on a 5083 aluminium alloy CT specimen.

is adopted. Here, the resolution is based on a finite element discretization supported by a mesh, taking 5-pixel square-shaped 4-node elements in a ROI of around 4000 × 800 pixels (see DIC parameters presented in Table 3). An example of the resulting displacement field calculated on an image captured during a FCG test (around the cycle $47 \cdot 10^3$) at $R = 0.1$ on a 5083 aluminium alloy CT specimen with respect to the reference image taken at minimum load before starting cycling loading, is shown on Fig. 6.

2.3.3. Crack opening displacement (COD) measurement

From the obtained DIC displacement fields, we can derive the crack opening displacement (COD) along the crack path for the 30 steps of each recorded cycle. The COD is a measure classically used in FCG tests to study the opening load P_{op}.

To evaluate the COD along the crack path on one displacement field $\underline{u}_y(\underline{x})$ (whatever the step), we compute the displacement difference dU_y between 2 horizontal lines spaced between 80 px and 200 px above and below the respective maximum and minimum y positions of the crack path (see an example in Fig. 7). By computing dU_y for the 30 steps within a cycle, the evolution of the COD along the crack is reconstructed over the loading cycle (Fig. 8 on the left side). We can also calculate the average COD profile along the crack path over a given cycle to analyze its evolution along the fatigue cycles, particularly during the lifetime of a multiplet, and compute the *Surface Contact Rate per cycle* (SCR, ranging from 0 to 1) For this purpose, a contact is defined as a local negative displacement measured between the 2 horizontal lines (defined above) of the displacement fields. Thus the *Surface Contact Rate per cycle* is calculated at each position along the crack path for a single cycle and corresponds to the counting of negative COD positions

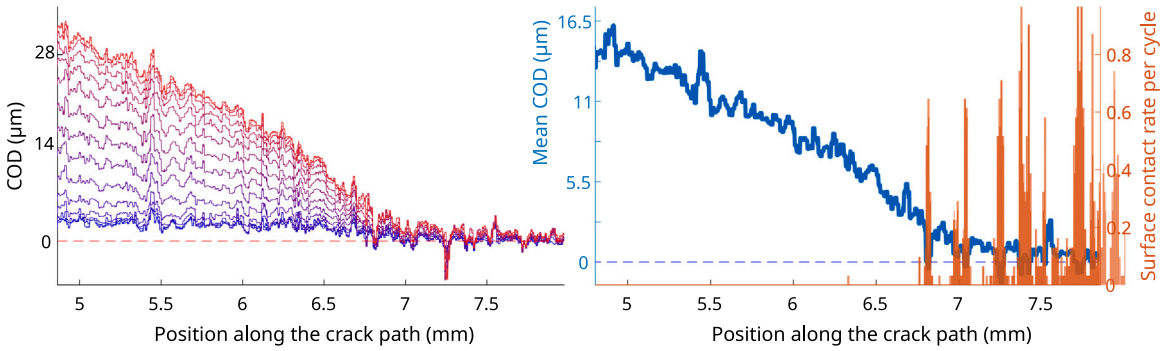

Fig. 8. Crack opening displacement analysis performed on images captured during a load-imposed FCG test at $R = 0.1$ on a 5083 aluminium alloy CT specimen. The origin of abscissa axis ($x = 0$) is set on the specimen notch tip. **Left** : CODs for 15 steps between the minimal load (blue) and the maximum load (red) of a cycle ; **right** : average COD profile over one cycle and the corresponding surface contact rate per cycle.

Table 4
Williams series parameters: expansion terms, material properties and projection zone sizes.

Terms	E	ν	R_{max}	R_{min}
$n \in [\![-3, 7]\!]$	70 GPa	0.29	0.413 mm	0.041 mm

over the 30 steps of this cycle. Then the total at each position along the crack path is normalized by the number of step in a cycle (30 steps). Fig. 8 presents an average COD profile over a cycle and the corresponding SCR.

2.3.4. *LEFM applied to displacement fields*

The crack tip position (CTP) and the stress intensity factor (SIF) can be estimated from the experimental displacement fields through a linear elastic fracture mechanics (LEFM) analysis. To apply LEFM, which assumes an isotropic homogeneous and elastic material, the plastic zone must be confined in a small domain around the crack tip. Since the plastic zone is large in the cyclic FCG tests performed on the aluminium alloy under study, for each multiplet, we subtracted the displacement field measured at minimum load of the cycle just before the emission of the first AE multiplet signal from any displacement field along the multiplet lifetime, to finally obtain a relative displacement fields.

This way, the relative displacement fields (30 per cycle during hundreds or even thousands of cycles) are freed from accumulated plasticity for the DIC calculation over the rest of the multiplet lifetime, allowing us to make a confined crack tip plasticity assumption over all these cycles. To ensure that this assumption is correct, CTP measurements for a fixed reference field at the beginning of the multiplet (field subtracted from all others along the multiplet lifetime) are compared to those for a variable reference field (minimum load fields of each cycle subtracted from each cycle). See Appendix for details on method, results and interpretation.

Then, to obtain the CTP and the SIF, the resulting relative displacement fields are projected onto the Williams' expansion (Eq. (2)) [24], an analytical solution for the stress distribution produced by a semi-infinite crack in an infinite homogeneous elastic solid with isotropic behavior [25].

$$\sigma_{ij} = \sum_{n} \sum_{p=I}^{II} A_p^n f_{ij}^{n,p}(\theta) r^{\frac{n}{2}-1} \tag{2}$$

where p is the loading mode, r and θ the polar coordinates (system centered on crack tip), $f_{ij}^{n,p}$ is a shape function depending on the stress tensor component σ_{ij} and A_p^n the Williams' expansion terms. For $n = 1$, the field is said to be singular because of the presence of a stress singularity for $r = 0$. The terms for $n < 0$ and $n > 1$ are respectively called super-singular and sub-singular terms. The super-singular terms are used to determine the position of the crack tip and the singular terms give the values of the stress intensity factors K_I and K_{II} (mode III not measured here). See Table 4 for Williams series parameters (here in plane strain conditions) and [26,27] for further details.

Since we are investigating relative displacement fields, for each multiplet m, we measure SIF ranges $\Delta K(t) = K(t) - K_{ref}^m$ over the cycles, where K_{ref}^m is the absolute value of the SIF of the field corresponding to the minimum load of the first cycle of multiplet m. Thus, for each multiplet m, K_{ref}^m is fixed throughout the lifetime of the multiplet (still, K_{ref} is neither measured nor computed). It should be noted that the measured SIF range $\Delta K(t)$ does not correspond to the classical notation $\Delta K = K_{max} - K_{min}$ as used in Paris' Law.

As the crack stays relatively straight during an experiment, we assume that the CTP takes values along a mean crack path line (white dashed line in Fig. 6). By this procedure, we obtain the CTP of an elastic equivalent crack that should correspond to the physical crack tip observed in displacements fields. Nevertheless, plasticity-induced crack closure means that the CTP, estimated as the position of an equivalent elastic crack tip by the procedure used here, is different from the actual physical crack tip. Thus, as

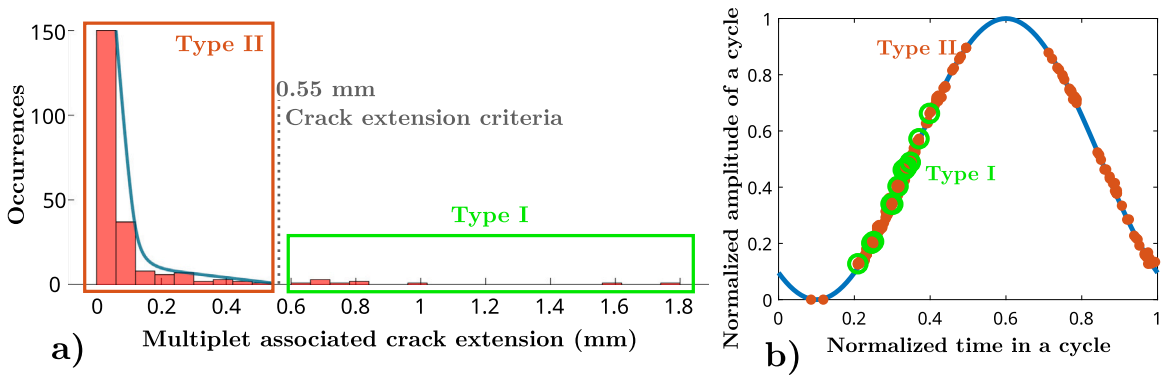

Fig. 9. Identification of type I and II multiplets using the *multiplet associated crack extension* criterion and mean multiplets emission loads. **(a)** Histogram of all multiplets associated crack extensions from fatigue crack growth experiments ($R = 0.1$ and $R = 0.7$) on aluminium alloy CT specimen. A small population of high crack extensions (green zone) is separated from a massive population of low crack extensions (red zone): a criterion $\delta_c = 0.55$ mm differentiates *Type I* multiplets from *Type II* multiplets. **(b)** The average load level at which type I (green circles) and II (orange dots) multiplets are recorded in a cycle (normalized).

approaching the end of a cycle coming back to the minimum load, the relative displacement fields return nearly in the same state as the reference image corresponding to the previous minimum load, the CTP steps back progressively from the tip to the back of the crack due to this plasticity effect. Consequently, when considering some cycles, the detected crack tip is going back and forth (see examples in Section 3).

2.4. AE and DIC synchronization

Although we implemented a triggering system to regularly capture 30 images within some loading cycles (see Section 2.3.1), the timestamps of the recorded images often suffer from a small delay relatively to the real acquisition instant due to the acquisition procedure and the relatively high solicitation frequency (5 Hz). Thus, an automatic synchronization of the image acquisition times to that of the AE signals is achieved by finding the maximum of the cross-correlation function between the two load measurements, one recorded by the AE system and the other by the image capture system

3. Results

Based on numerous tests under different loading conditions (presented in Section 2.1), the acoustic multiplets were classified by our algorithm, briefly explained in 2.2.2 and fully detailed elsewhere [21]. We checked that the sources of the multiplet signals were neither noise nor originating from far from the crack: all multiplets recorded by both sensors have a source located along the crack path (mean distance between the two sensors, see Fig. 5). Hence, the first observation is that the recording of a multiplet does reveal the presence of a crack. However, the reciprocal is not true as no multiplet are recorded during a large number of cycles of the crack propagation phase. It is important to note here that, for a given multiplet, there is in principle one AE signal per cycle, occasionally interrupted by *silent zones* during which the multiplet signal is temporarily lost, most likely due to SNR problems (see [21] for further details), which means that a multiplet m of N_m signals lasts at least N_m cycles. Finally, we also see that all different sensors have detected the same multiplets. According to the different sensibilities and sensor positions, some signals in multiplets have been missed, especially for the *micro 200* (wide-band sensor) but it does not represent a significant part of total signals. Thus, as there is no qualitative difference between the 3 sensors detected multiplets, we do not distinguish the sensors in the rest of the paper. Next, the combined AE and DIC analyses performed during the lifetime of these detected multiplets showed two clearly different types of acoustic multiplets.

3.1. Multiplets typology

3.1.1. Distinction between two types of multiplets based on their associated crack extension

Thanks to the synchronization of AE and DIC, providing times of emission t_i^m (m being the multiplet number and i the ith signal within multiplet m) and the corresponding crack tip position $a(t_i^m)$, we can measure, for each multiplet, the associated crack extension occurring during the multiplet duration, referred to as the *multiplet associated crack extension* $\delta_m = a(t_{N_m}^m) - a(t_1^m)$, where N_m is the number of signals in multiplet m. From Fig. 9**a** representing an histogram of all δ_m obtained from our experimental dataset, we can distinguish a few outliers, namely δ_m-values greater than 0.5 mm (green rectangle in Fig. 9), from the rest of the distribution corresponding to smaller associated crack extensions (red rectangle). We therefore selected a threshold value of 0.55 mm to separate these two domains. Thus, by setting a criterion $\delta_m > \delta_c = 0.55$ mm we extract a small cluster of multiplets called *Type I multiplets* from the rest of the multiplets dataset thus called *Type II multiplets*.

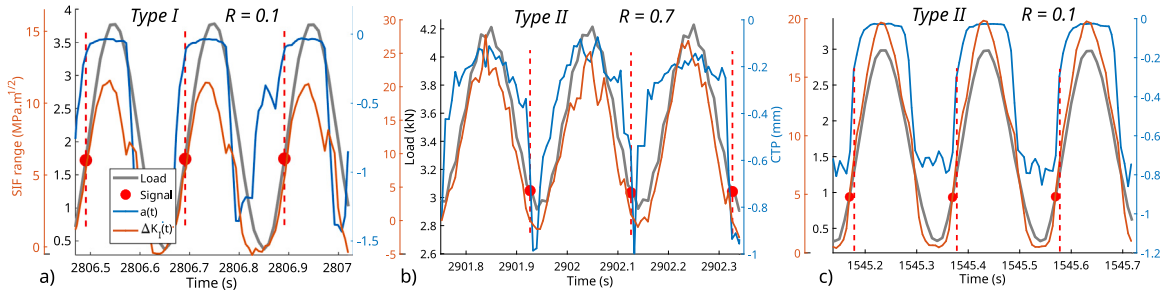

Fig. 10. Stress intensity factor range (orange), crack tip position (blue) and applied load (gray) measurements during the first cycles of three distinct acoustic multiplets, each emitted during an FCG test on a 5083 CT aluminium specimen : **(a)** Type I multiplet during a $R = 0.1$ experiment, **(b)** type II multiplet during a $R = 0.7$ experiment, **(c)** type II multiplet during a $R = 0.1$ experiment. The red dots indicate the occurrences of the multiplet signals and the vertical red dashed lines are indicators of t_i to help the eye to see $CTP(t_i)$ values (note that the CTP values are only used to show the backward movement of the detected crack tip and cannot be compared with each other on the three graphs).

We can then depict the characteristics of the two groups:

- *type I* multiplets with large δ_m, larger than one or several millimeters, very few occurrences recorded only during the first half of the specimen lifetime.
- *type II* multiplets with much smaller δ_m, below ~500 µm, large number of occurrences.

Note that although type I multiplets could be considered as outliers in terms of statistics (Fig. 9**a**), they are not AE artifacts as these multiplets are composed of thousands of signals satisfying the multiplets definition requirements.

In addition, by looking at type I and II occurrences in our experiments, we find that type I multiplets are only recorded during experiments performed under a small load ratio $R = 0.1$, whereas type II are observed during all experiments. Moreover, by plotting the average load level at which type I and II multiplets are recorded over a normalized cycle (Fig. 9**b**), we observe that type I multiplets are always emitted during loading ($\dot{P} > 0$), while type II are emitted at almost all load levels for both loading and unloading (except near maximum load).

Nevertheless, as type I occurrences are mixed with type II ones in Fig. 9**b**, it shows that it is not possible to recognize type I from type II only by the multiplets emission load levels or loading/unloading phase distinction. That is the reason why we investigate multiplets signals emission within cycles through an AE-DIC synchronized analysis.

3.1.2. Distinction based on crack tip position

The synchronized analysis between AE and DIC measurements provides an information on stress and displacement states around the crack at the emission of a multiplet signal, as well as the associated CTP. Measuring the CTP over a few cycles at the beginning of multiplets, and relating it to the multiplet emissions within the loading cycle, allows to distinguish opening or closing phases of the crack observed by DIC on the surface. As we have assumed a rectilinear crack trajectory in our analysis (see 2.3.4), the CTP returns to a 1D position over this path.

The reference of CTP measurements ($CTP = 0$) is arbitrarily defined and lacks physical significance, restricting the comparison of CTP curves among the depicted graphs.

The Fig. 10 illustrate the CTP $a(t)$, the SIF range $\Delta K_I(t)$ and the cyclic loading, for typical examples of type I (10**a**) and type II (10**b** and **c**) multiplets. The resulting CTP $a(t)$ of the equivalent elastic crack shows a plateau at maximum crack opening, preceded by a rise and followed by a descent due to plasticity (see 2.3.4 for more details). The CTP measurement reference (value $CTP = 0$) is user-defined at the crack guide's origin, coinciding with the maximum visible crack extension, but lacks physical meaning. Consequently, CTP curves solely indicate the backward movement of the detected tip and are not comparable across the three graphs. Occurrences of multiplet signals are indicated by red dots. The vertical red dashed lines help the eye to determine the values of SIF $\Delta K_I(t_i^m)$ and CTP $a(t_i^m)$ at the emission of signal i of multiplet m. Note that the cyclic behavior of the CTP is less pronounced for $R = 0.7$ (Fig. 10**b**) and do not show a plateau as the $R = 0.1$ case (Fig. 10**c**), since the crack remains essentially open.

The combined AE-DIC analysis performed on different multiplets reveals a clear distinction between types I (Fig. 10**a**) and II (Fig. 10**b** and **c**) on CTP curves. Type I multiplets have a specific behavior: the first signals appear at the beginning of the CTP plateau, and start to appear increasingly sooner during the rise of the CTP curve. In contrast, type II multiplets do not display this consistent behavior or any other observable pattern. (Fig. 10**b** and **c**). The conceptual sketch in Fig. 11 summarizes typical type I multiplets behavior along their lifetimes. However, it should be noted that some multiplets classified in the type II group show the same behavior as the type I described here by the synchronized AE-DIC analysis. Indeed, due to signal-to-noise ratio issues and AE amplitude variations in multiplet signals, which cause *silent zones* during a long multiplet (see [21] for more details), the automatic multiplet classification explained in Section 2.2.2 can sometimes separate a single long multiplet (such as type I multiplets) into several smaller parts. These portions, originating from a single multiplet, are then considered as different multiplets and each have smaller associated crack extensions δ_m, resulting in erroneous extraction according to the δ_c criterion, defined in Section 3.1.1. From this perspective, we have identified these errors on type II multiplets as belonging to type I.

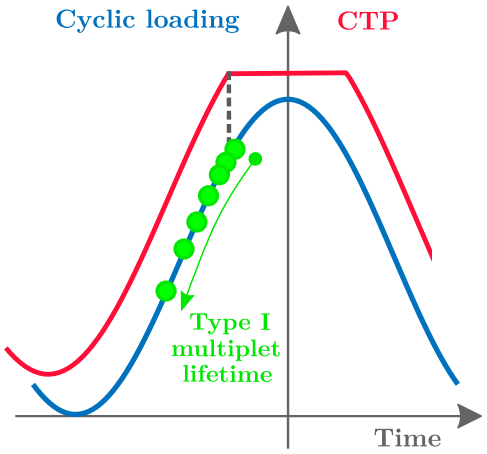

Fig. 11. Schematic representation of the charge levels at which signals of **type I** multiplets are recorded, cycle after cycle, in correspondence with the position of the crack tip (CTP). The red curve is representative of the crack tip position over the lifetime of the multiplet (varies very little over the lifetime). Green dots are some multiplet signal occurrences plotted on the load cycle (one signal corresponds to one cycle): signals at the start of the multiplet are synchronized with the onset of the CTP plateau, and then appear increasingly earlier than the onset of this plateau.

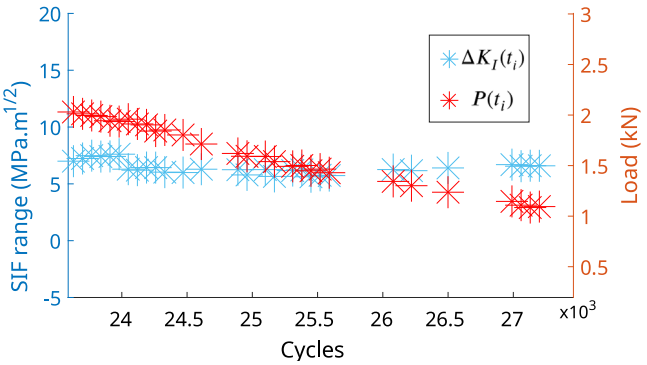

Fig. 12. Evolution of a **type I** multiplet emission load $P(t_i)$ and stress intensity factor range $\Delta K_I(t_i)$ calculated every 50 cycles during a FCG test ($R = 0.1$) on aluminium 5083 CT specimen. The entire lifetime of the multiplet is covered by this analysis.

Therefore, we can conclude that the CTP measured from DIC, synchronized with AE multiplet detection, provides an even more efficient way to separate type I multiplets from type II multiplets, consistent with the criterion based on the associated crack extension of these multiplets, explained in Section 3.1.1 (some exceptions, detailed above, aside).

Finally, it is important to note that these two types of multiplets cannot be distinguished based on classical AE descriptors. Indeed, we performed a principal component analysis to search for latent variables able to differentiate type I from type II signals within a dataset, without success: no combination of descriptors can achieve this. This reinforces the interest of the approach proposed here.

3.2. Investigation of the two types of multiplets

3.2.1. SIF range and CTP evolution during type I multiplets

Since the crack extension δ_m associated with type I multiplets is large, we can track the evolution of $\Delta K_I(t_i^m)$ and $a(t_i^m)$ over their lifetime ($i \in [1, N]$) by performing the same analyses explained in Section 2.3.4 on some separated cycles of the same multiplet, distributed throughout its lifetime.

Fig. 12 represents the evolution of $\Delta K_I(t_i^m)$ and $P(t_i^m)$, the SIF range and load values associated with the signal i of a multiplet m of type I. It can be seen that the multiplet evolution is straightened by representing the stress intensity factor range ΔK_I values at emission t_i^m instead of the load values P at the same instant. This constant trend of SIF range $\Delta K_I(t_i^m)$ measured at type I multiplet emissions is always observed for the smallest type I multiplets, i.e. with a low δ_m around 0.6 mm, as well as for very long type I multiplets with $\delta_m > 4$ mm.

As explained in Section 2.3.4, all SIF ranges for a multiplet m are calculated from the same displacement field reference K_{ref}^m taken at the minimum load of the cycle at the multiplet onset. Since $\Delta K_I(t) = K_I(t) - K_{ref}^m$ with a constant K_{ref}^m, the relative measured evolution of $\Delta K_I(t_i)$ (over all multiplet signals i emissions) is equal to the absolute SIF $K_I(t_i)$ evolution over the multiplet lifetime.

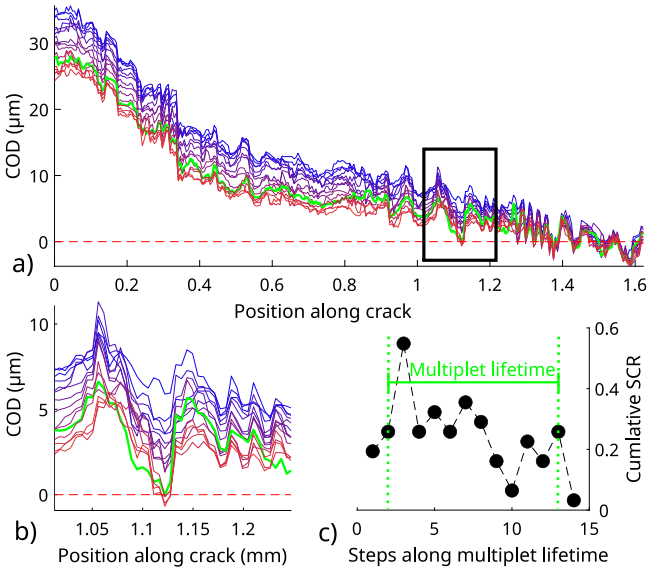

Fig. 13. **(a)** Crack opening displacement profiles along the crack path extracted from 15 displacement fields, from the maximum load (blue curves) to the minimum load (red curves) during the **unloading** phase of a cycle when a **type II** multiplet signal was emitted, for a test performed on a 5083 aluminium CT specimen ($R = 0.7$). The green curve corresponds to the emission of a type II multiplet signal. **(b)** Zoom over the black box, showing that the AE multiplet is emitted at the time of local contacts of crack surfaces. **(c)** Evolution of *cumulative surface contact rate (SCR)* over $[1.05; 1.15]$ mm of the crack path (i.e. dark box in **(a)**) during the multiplet lifetime. Steps are single non-consecutive cycles studied before, during and after the multiplet lifetime. From the beginning to the end of the multiplet lifetime, the cumulative SCR decreases overall until it reaches approximately 0 (no contact).

In conclusion, we can say that type I multiplets signals occur at constant stress intensity factor $K_I(t_i^m)$ while their emission load levels $P(t_i^m)$ decrease, all along their lifetimes.

3.2.2. Results of the COD analysis

Type II multiplets A detailed examination of our COD analysis allows us to associate the emission of type II multiplets occurring during the unloading phase with a local crack surfaces contact mechanism. When multiplets signals are emitted far from the CTP plateau, the values of $\Delta K_I(t_i^m)$ and $a(t_i^m)$ are not well determined as the crack appears to be closed. Let us recall the major difference between the COD analysis, which is performed relatively to an absolute reference (image taken before the start of cyclic loading), and the CTP or SIF measurements, which are performed on relative references (relative displacement fields). In these situations, the calculation of COD profiles reveals contacts between the two cracks surfaces (at least on the specimen face seen by the camera), along the crack path and behind the crack tip (example in Fig. 13). By synchronization of the AE and COD analyses, we are able to associate the emission of multiplet signals with a COD profile during unloading (green curve in Fig. 13). This highlights a correlation between such local contacts of crack surfaces and the emission of multiplets.

More specifically, we found that COD profiles associated with the emission of several type II multiplets correspond to the onset of crack surfaces contacts at the level of some asperities (COD≤0). This is illustrated, for example, in Fig. 13**b**, with the green curve corresponding to the multiplet emission as well as to the onset of crack surfaces contacts at $x_m = 1.12$ mm. To go a step further, this type of analysis can be conducted over the entire multiplet duration: Fig. 13**(c)** shows a decrease in *cumulative surface contact rate* (SCR summed over a short portion of crack path), which is a measure of contact intensity along the multiplet lifetime. In other words, the crack surfaces contacts at this asperity and the multiplet emission fade simultaneously, arguing in favor of their association. Later in the test, far after the end of the multiplet, no contact was detected at this position along the crack path. This phenomenon is observed for several type II multiplets emitted not only during unloading or around the minimum load but also during loading. In addition, quite surprisingly, crack surfaces contacts are also observed for tests performed with a $R = 0.7$ loading ratio, as for $R = 0.1$ experiments.

Type I multiplets A same COD analysis is performed during type I multiplets lifetime. An example is shown in Fig. 14, which contains COD curves for two cycles taken at different times around beginning (Fig. 14**a**) and end (Fig. 14**b**) of the multiplets lifetime. These graphs suggest that, unlike type II multiplets, type I multiplets are not linked to local crack surfaces contacts behind the crack tip, since the green curves never reach $COD = 0$. Furthermore, with regard to a contact close to the tip where the accuracy of the COD measurement is not sufficient to conclude, the comparison between Fig. 14**a** and **b** shows nevertheless that no hypothetical contact close to the crack tip (around $x \in [2; 2.5]$ mm) in state **a** persists in state **b** while the multiplet continues to emit.

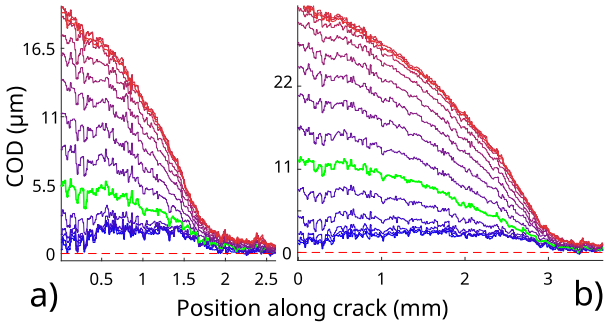

Fig. 14. Crack opening displacement along the crack path extracted from 15 displacement fields, from the minimum load (blue curves) to the maximum load (red curves) during the **loading** phase of the cycle, for a FCG test ($R = 0.1$) on a 5083 aluminium CT specimen. Green curves correspond to the emission of a **type I** multiplet signal. **(a)** and **(b)** are cycles taken at separate times around respectively beginning and end from multiplet lifetime.

4. Discussion : interpretation of physical sources and mechanisms for the two types of multiplets

The results presented above provide information about the physical sources of the acoustic multiplets, which appear as specific acoustic signatures of a fatigue crack. By signature, we do not mean a specific waveform identifiable from time or frequency domain features as often proposed in the literature (AE energy [15], Rise angle [28], frequency peaks [16], waveforms information entropy [17,29]), but the multiplet itself as defined in introduction (Section 1.3).

The significant differences between the two types of multiplets revealed by our synchronized AE and DIC analysis suggest a specific source mechanism for each type. We begin with a fairly straightforward explanation of the source mechanisms for type II multiplets. We then demonstrate that type I cannot share the same physical source, and propose an interpretation for the emission of these type I multiplets.

4.1. Type II multiplet source mechanism: local rubbing over fracture surfaces

The COD analysis presented in Fig. 13 demonstrates that the emission of type II multiplets is associated with crack surface contacts on a local asperity during unloading or loading, implying frictional contacts, even when the test is carried out under a load ratio of $R = 0.7$, for which a crack is often considered to be always opened. These local crack surface contacts may occur, under these traction-traction loading conditions ($R = 0.7$), on asperities along rough crack paths, known as *Roughness-induced crack closure* [30]. To confirm this, post-mortem SEM fractographic observations were made around the positions, along the crack path, of crack surface contacts detected by our COD analysis.

Fig. 15 shows SEM images of the crack surface of the specimen which emitted the type II multiplet studied in Fig. 13. First, a global view is shown on the left to identify the area around the position of crack surface contact $x = 1.12$ mm along the crack path (position identified in Fig. 13). Then, at this position, close to the specimen free surface, in front of the camera view (top of the SEM image), we found a squashed area (see the zoomed SEM image on the right of Fig. 15). Note that, with the exception of another small flattened surface inside the specimen, on the left of Fig. 15, we found no other signs of crack surface squashing in this specimen.

This correspondence between the triggering of a type II multiplet, the detection of local crack closure from the DIC analysis, and the presence of local squashing, has been observed a few times in our experiments. However, if local crack closure occurs within the specimen, far from its free surfaces, it cannot be detected by the DIC analysis while still emitting a repetitive AE signal at each loading cycle when rubbing occurs. We therefore argue that these type II multiplets correspond to rubbing events over the crack faces. Consequently, they can be observed during loading or unloading, but never around the peak load (see Fig. 9**b**). Their associated crack extension is always limited (Fig. 9**a**, as those local contacts are lost when the crack front advances and the crack surface geometry is modified.

As a result, the detection of these Type II AE multiplets enables the non-destructive in-operando detection of friction along fracture surfaces, and thus the detection of the presence of a crack. Moreover, following this interpretation, a detailed analysis of the characteristics of the associated AE waveforms could be potentially used to deduce information about the source, such as its size or the evolution of roughness-induced crack closure (not studied here).

4.2. Type I multiplets source mechanism

During the lifetime of type I multiplets, cracks propagate over distances δ_m ranging from ~500 μm to a few millimeters (see Section 3.1 and Fig. 9**a**). Furthermore, type I multiplets are always recorded when the two crack faces are well separated, as indicated by the COD analysis (see e.g. Fig. 14). In our opinion, this rules out the possibility of a friction-related mechanism as a possible source of these multiplets.

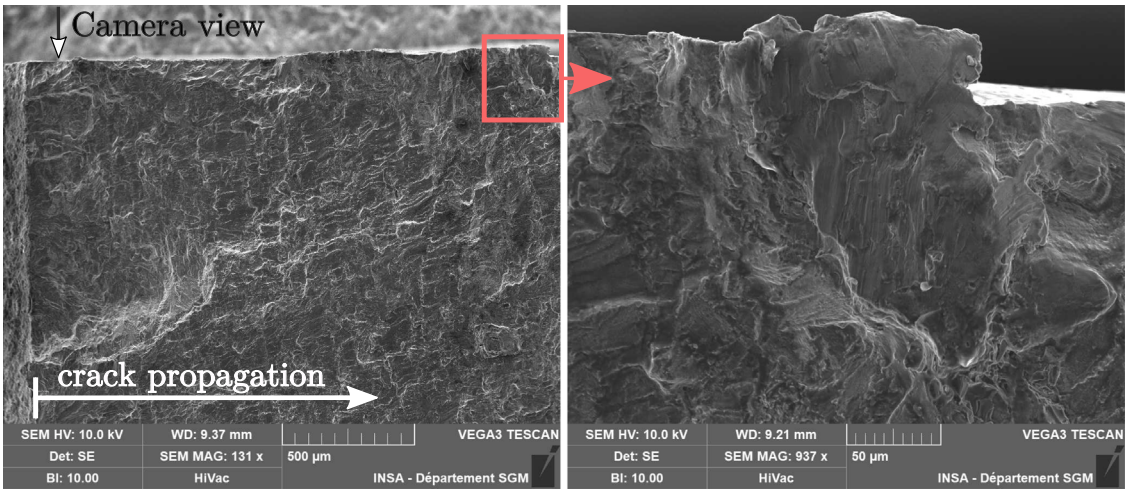

Fig. 15. Post-mortem SEM fractographies of a 5083 aluminium alloy CT specimen loaded in fatigue at $R = 0.7$. The right image is a zoom over the red square, showing squashing of the crack surfaces, close to the specimen surface, in front of the camera view. The contact site identified by the COD analysis in Fig. 13 allowed us to find this squashed area.

4.2.1. A crack propagation mechanism at crack tip

Therefore, in absence of crack surfaces contact (possible source behind the crack tip) and given that 1D acoustic location shows that the sources of these type I multiplets are spatially located along the crack path over the cycles (see e.g. Fig. 5), we can conclude that their source mechanism occurs at the crack tip and progresses with it as the extended *associated crack extension* suggests.

As widely admitted, crack propagation, including in cyclic fatigue, is driven by the stress intensity factor at crack tip. Thus, since type I multiplets are physically emitted near the crack tip, at a constant SIF $K_I(t_i^m)$ (see Section 3.2.1) throughout their lifespan, (while the applied load at emission $P(t_i^m)$ decreases) and, for the first signals, at the onset of the CTP plateau, they can be associated with a crack propagation mechanism at the crack tip, occurring, cycle after cycle, as the crack reopens. This result means that type I multiplets can be considered as an acoustic signature of incremental crack propagation. This is a key result of the present work in terms of non-destructive detection and fatigue monitoring.

Yet, type I multiplet signals do not all occur at the onset of the CTP plateau (corresponding to crack opening), which requires further investigation.

4.2.2. Differentiated internal and external crack opening

As the DIC measurements are performed only on a specimen free surface, the SIF range estimation and crack tip detection refer only to the crack behavior at this external surface. Consequently, their values in the thickness of the specimen are unknown. Moreover, the location of the AE source within the thickness remains unknown as well.

From the works of Elber [31] and Schijve [32], we have an idea of the variations of crack opening throughout the sample thickness due to plastic effects. Indeed, the outer part of the crack (near free surfaces) is subjected to plane stress conditions, while the inner part is subjected to plane strain conditions. In addition, we know that the plastic zones at crack tip have different sizes under these two conditions, $r_{plane-stress}$ and $r_{plane-strain}$ [33,34]:

$$r_{plane-stress} = \frac{1}{\pi}\left(\frac{K_I}{\sigma_y}\right)^2 \tag{3}$$

$$r_{plane-strain} = \frac{1}{3\pi}\left(\frac{K_I}{\sigma_y}\right)^2 \tag{4}$$

where σ_y is the yield strength of the material.

Under plane stress conditions, the plastic zone at crack tip is therefore three times larger than under plane strain conditions [35]. The resulting residual stresses are therefore greater near the free surfaces of the specimen (outer parts of the crack) compared to the specimen core (inner part of the crack), implying that the fatigue crack remains closed over a larger part of the loading cycle at the edge of the specimen than inside [34]. Indeed, smaller residual stresses inside the specimen mean that the load P_{op}^{in} required to open the inner part of the crack is lower than the load P_{op}^{out} required to open the outer parts. We can therefore conclude that, during a cycle, when P reaches P_{op}^{in}, the inner part of the crack opens first, eventually leading to the emission of a multiplet signal, while the outer parts open later at P_{op}^{out}. This phenomenon is schematically represented in Fig. 16.

This means that the crack opening may occur inside the sample before a full opening is detected by the DIC with the onset of the CTP plateau. Therefore, a type I multiplet emitted in the specimen core may be linked to a crack propagation mechanism at crack tip even if the associated AE signals are recorded before reaching the CTP plateau (as seen from the DIC on CTP curves).

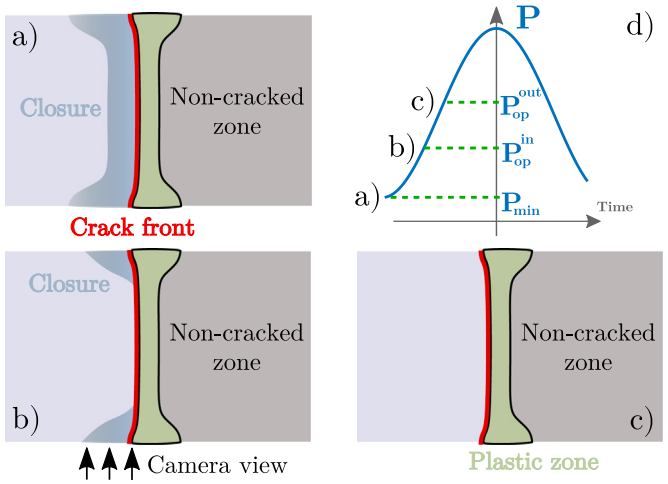

Fig. 16. Schematic representations of fatigue crack opening along thickness during a load cycle. **(a)**, **(b)** and **(c)** are successive crack opening states (crack is advancing from left to right): **(a) Maximum closure** at minimum load P_{min} **(b) Inner crack opening** at load P_{op}^{in}. **(c) Outer crack opening** at load P_{op}^{out}. **(d)** A loading cycle showing succession of minimal and opening loads.

4.2.3. Increased difference between inner and outer crack opening loads during crack propagation

Let us recall that we observe a progressive shift of signal occurrences on the CTP curve: type I multiplet signals are synchronized, at the beginning of the multiplet, with the onset of the CTP plateau – complete crack opening –, and then appear earlier and earlier. This specific behavior of type I multiplets (discussed in Section 3.1 and shown in Fig. 9) can be explained by the gap between the inner and outer crack opening loads, which itself becomes increasingly larger as the crack propagates. Indeed, the difference in the size of the plastic zones $r_{plane-stress} - r_{plane-strain}$, and hence the resulting difference in residual stresses, increases as the square of K_I. This implies that the difference between P_{op}^{out} and P_{op}^{in} is unnoticeable at the beginning of the crack propagation and increases rapidly as the crack propagates. This may explain the progressive de-synchronization between the CTP surface measurement and the multiplet emission, whose physical source may be located in the thickness of the specimen.

4.2.4. Type I multiplets emitted at constant SIF along the specimen thickness

Since we only perform a surface measurement of the SIF range and we consider a different behavior for the inner and outer parts of the crack, we may wonder whether the constant SIF range observed (at the free surface) can be associated to type I multiplets emitted within the sample's thickness.

From the literature [2,34,36], it appears that the SIF values at the free surfaces are much greater than those at the center of the specimen. However, a numerical analysis of the through-thickness distribution of the effective SIF range for compact tension specimens under test conditions similar to our own (CT geometry, $R = 0.1$, material constants) [36] shows that the difference $\delta K_{max}(a) = K_{max}^{out}(a) - K_{max}^{mid}(a)$ between the SIF at the surface K_{max}^{out} and at median plane K_{max}^{mid} remains very small during the first millimeters of propagation from the CT notch. Thus, for a type I multiplet emitting signals at times t_i, a constant $\Delta K_I^{out}(t_i)$ trend (measured) characterizes also a constant $\Delta K_I^{in}(t_i)$ trend, which are both directly associated respectively to constant $K_I^{out}(t_i)$ and $K_I^{in}(t_i)$. This is in full agreement with the association of type I multiplets to a crack propagation mechanism as explained in Section 4.2.1.

4.2.5. Verification of plane strain and plane stress conditions in our specimen

The above discussion about the delayed opening of the outer parts of the crack is based on the coexistence of plane stress and plane strain conditions during type I multiplets emission. In some of our experiments exhibiting type I multiplets, the confirmation of mixed mode occurs through the observation of shear lips on the post-mortem crack surfaces. These shear lips initially emerge close to the free surfaces of the specimen (plane stress conditions) and progressively extend inward (plane strain) as the crack propagates [32,33]. To highlight the presence of increasing shear lips on the crack surfaces, we performed a 3D fractography revealing the roughness of the fracture surface, from the CT notch (left-hand side of Fig. 17) to half the total crack extension (right-hand side) of a $R = 0.1$ test. The corresponding type I multiplet crack extension is framed in dark red in Fig. 17 to show the correlation between shear lips and the onset of the multiplet. Shear lips formation is a consequence of the transition from plane strain to plane stress described above, and shear lips size can even be considered as a measure of the plane stress plastic zone size $r_{plane-stress}$ [37]. Furthermore, shear lips are known to produce increasing crack closure along the thickness during crack propagation, which is entirely consistent with the interpretation of the type I source mechanism given above. Note that the emission of type I multiplet is not consistently linked to the presence of shear lips. In certain experiments, type I multiplets have been recorded without the observation of shear lips (but with strong 3D structures and debris), and conversely, experiments with a stress ratio of $R = 0.7$ have shown limited shear lips despite the absence of type I multiplet recorded.

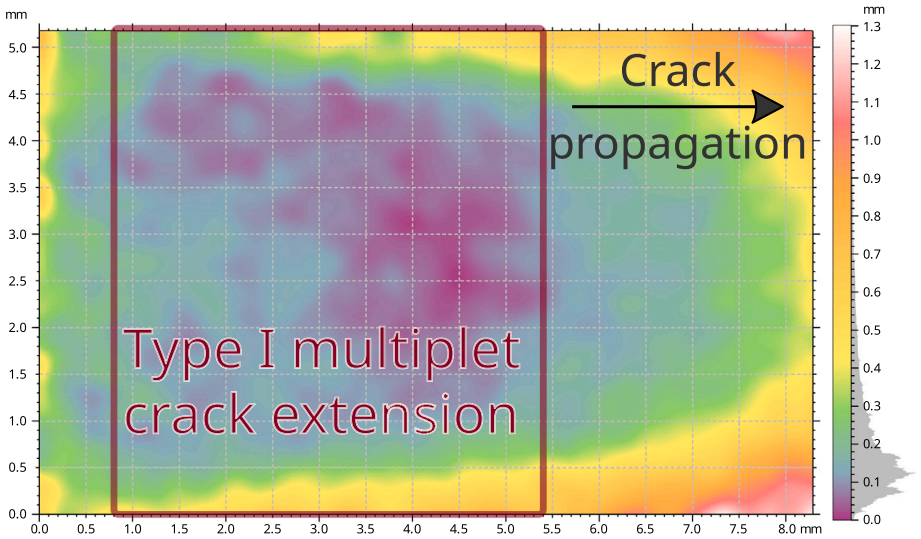

Fig. 17. 3D fractography of a post-mortem fracture surface for a load-imposed $R = 0.1$ experiments on a 5083 aluminium alloy CT specimen. The corresponding type I multiplet crack extension is framed in dark red to show the correlation between shear lips and the onset of the multiplet.

4.2.6. An AE source mechanism associated to crack propagation

The combined analysis of AE multiplets and synchronized DIC (crack tip detection, COD measurement and SIF estimation) has enabled us to associate the emission of type I multiplets with a crack propagation mechanism at crack tip. We now discuss the exact nature of the physical source of type I multiplets signals by proposing 3 hypothesis in descending order of certainty.

In the literature [7,38,39], AE signals occurring at the crack opening near the crack tip, during fatigue, have been proposed to originate from an extension of the plastic zone, i.e. dislocation motion, and/or from crack extension. Considering that type I multiplets are emitted neither during tests at $R = 0.7$ nor in the second half of a test at $R = 0.1$, we suggest that type I multiplets could be due to the re-activation of plasticity at crack tip after reverse plastic deformation during unloading, which may happen in the first part of $R = 0.1$ experiments when the crack is sufficiently short. As the cracks always remain open in the $R = 0.7$ experiments, there is no reverse plasticity in this case, and in the $R = 0.1$ experiments, as K_I increases more and more rapidly (both at maximum and minimum load) as the crack propagates, reverse plastic deformation is less and less pronounced. This re-activation of plasticity at each cycle would occur naturally at a constant SIF as type I multiplets do.

Another hypothetical physical mechanism for type I multiplets could be cleavage-like and/or intergranular-like microcracking [38–40], particularly under triaxial stresses [39,40] which are known to favor impulsive AE signals. Indeed, although our CT specimens are, in principle, solicited in mode I, mixed mode cracking (modes I, II and III) may occur locally, like in shear lips (see Section 4.2.5), during crack propagation at free surfaces or in the specimen core, creating type I multiplets sources resulting from a cracking mechanism under triaxial stresses.

Lastly, there could be another explanation for the physical mechanism behind type I multiplets. It involves friction on the crack surfaces during the opening phase at the end of the opening process, particularly on sharp 3D variations. This could be supported by the presence of minor debris in the vicinity of the locations where type I multiplets are emitted on the specimens.

5. Conclusion

The synchronized DIC and AE analyses of fatigue crack propagation tests conducted in this study revealed the existence of two distinct types of acoustic multiplets. These types were identified through two separate methods, both relying on DIC measurements, and are characterized by their unique source mechanisms.

Detailed DIC analyses showed that type II multiplets are the consequence of local contacts, repeated at each cycle, of the crack surfaces, while multiplets of type I, emitted at a constant stress intensity factors, are associated with a propagation mechanism at the crack tip. In other words, type II multiplets are a signature of the *presence* of a fatigue crack that can be detected in volume. Type I multiplets serve as a distinctive indication of the *propagation* of a fatigue crack: their source, located at the crack tip, moves forward in conjunction with the crack, in contrast to type II multiplets, which are linked to a fixed source. We delve into the specific physical mechanism behind the emission of these type I signals, and our interpretation suggests that they likely result from the reactivation of plasticity at each cycle, following reverse plastic deformation at discharge.

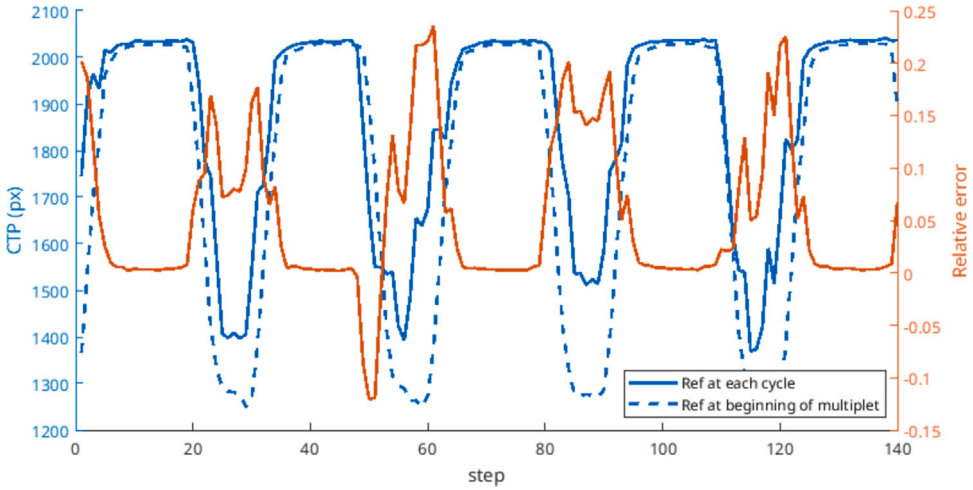

Fig. 18. CTP measurements (dashed and solid blue curves) using two *reference* fields: a single field taken at the onset of the multiplet (dashed) and fields at the minimum loads of each cycle (solid). The relative error between these two curves is represented in orange.

CRediT authorship contribution statement

Théotime de la Selle: Writing – review & editing, Writing – original draft, Software, Methodology, Investigation, Formal analysis, Conceptualization. **Julien Réthoré:** Validation, Software, Investigation, Conceptualization. **Jérôme Weiss:** Writing – review & editing, Validation, Supervision, Conceptualization. **Joël Lachambre:** Validation, Software, Methodology. **Stéphanie Deschanel:** Writing – review & editing, Validation, Supervision, Project administration, Investigation, Conceptualization.

Declaration of competing interest

The authors declare that they have no known competing financial interests or personal relationships that could have appeared to influence the work reported in this paper.

Data availability

Data will be made available on request.

Acknowledgments

This research was funded, in whole or in part, by the Agence Nationale de la Recherche (ANR) through grant ANR-19-CE42-0012. A CC-BY public copyright license has been applied by the authors to the present document and will be applied to all subsequent versions up to the Author Accepted Manuscript arising from this submission, in accordance with the grant's open access conditions.

Appendix. Validation of the CTP and ΔK_I measurement method

To eliminate the accumulated plasticity at the crack tip in this field measurement — since the projected model is purely elastic — we subtract the displacement field at the minimum load of the cycle preceding the appearance of the multiplet (referred to as the *reference* field) from all measured displacement fields throughout the life of a multiplet. This results in relative displacement fields.

However, type I multiplets may be associated with significant crack growth, raising questions about the validity of the confined plasticity assumption for all relative displacement fields until the end of the multiplet.

To ascertain this, a similar measurement of CTP and SIF is conducted using relative displacement fields where the subtracted field varies with each new cycle (image taken at the minimum load of the studied cycle). In this case, the accumulated plasticity at the crack tip during a cycle is sufficiently low. We consider the most unfavorable situation: the greatest crack growth associated with the lifetime of a multiplet (crack several millimeters long) whose fields are analyzed at the end of its life. CTP measurements for a fixed *reference* field, taken at the beginning of the multiplet (field subtracted from all others) are compared with those for a variable *reference* field (minimum load fields of each cycle subtracted from each cycle). The curves are shown in Fig. 18. The relative error is also displayed.

The cyclic behavior of CTP curves is observed, with plateaus at each loading period corresponding to moments when the crack is fully open (see Section 3.1.2). The backward and forward movement of the crack tip in each cycle is due to plastic effects: the

equivalent elastic crack becomes less and less representative of the physical crack in the displacement fields. It is thus logical that CTP measurements on these crack opening–closing portions differ depending on the reference field used. It is therefore more appropriate to compare CTP measurements calculated during plateaus to assess the impact of a single reference at the beginning of the multiplet. Moreover, we observe that at the plateau, the relative error drops and almost cancels out, showing that our two measurements do not significantly differ, and thus that the plasticity accumulated at the crack tip throughout the life of type I multiplets does not affect our measurements significantly. Consequently, our measurement of CTP, and therefore of $\Delta K_I(t)$, performed from a fixed reference field at the minimum load of the cycle preceding the multiplet appearance, is reliable throughout the life of type I multiplets.

References

[1] Schütz W. A history of fatigue. Eng Fract Mech 1996;(54):263–300.
[2] Suresh S. Fatigue of materials. 2nd ed.. Cambridge university Press; 2001.
[3] Schijve Jaap. Fatigue of structures and materials. 2nd ed.. Dordrecht: Springer; 2010.
[4] Wood WA. Formation of fatigue cracks. Phil Mag : J Theor Exp Appl Phys 1958;3(31):692–9.
[5] Paris P, Erdogan F. A critical analysis of crack propagation laws. J Basic Eng 1963;85(4):528–33.
[6] Harris DO, Dunegan HL. Continuous monitoring of fatigue-crack growth by acoustic-emission techniques: Purpose of this investigation was to further explore the relationship between crack-growth characteristics and acoustic-emission variables such as instrumentation gain and sensor frequency. The threshold conditions for crack detection were also investigated. Exp Mech 1974;14(2):71–81.
[7] L'Hôte G, Cazottes S, Lachambre J, Montagnat M, Courtois P, Weiss J, Deschanel S. Dislocation dynamics during cyclic loading in copper single crystal. Materialia 2019;8:100501.
[8] Weiss J, Rhouma W Ben, Richeton T, Dechanel S, Louchet F, Truskinovsky L. From mild to wild fluctuations in crystal plasticity. Phys Rev Lett 2015;114(10):105504.
[9] van Bohemen S M C, Hermans M J M, den Ouden G, Richardson I M. A study of acoustic emission energy generated during bainite and martensite formation. J Phys D: Appl Phys 2002;35(15):1889–94.
[10] Shaira M, Godin N, Guy P, Vanel L, Courbon J. Evaluation of the strain-induced martensitic transformation by acoustic emission monitoring in 304L austenitic stainless steel: Identification of the AE signature of the martensitic transformation and power-law statistics. Mater Sci Eng A 2008;8.
[11] McBride SL, MacLachlan JW, Paradis BP. Acoustic emission and inclusion fracture in 7075 aluminum alloys. J Nondestruct Eval 1981;2(1):35–41.
[12] Rouby Par D, Fleischmann P, Duvergier C. Un modèle de sources d'émission acoustique pour l'analyse de l'émission continue et de l'émission par salves I. Analyse théorique. Phil Mag A 1983;47(5):671–87.
[13] Roberts TM, Talebzadeh M. Acoustic emission monitoring of fatigue crack propagation. Journal of Constructional Steel Research 2003;59(6):695–712.
[14] Berkovits Avraham, Fang Daining. Study of fatigue crack characteristics by acoustic emission. Eng Fract Mech 1995;51(3):401–16.
[15] Chai Mengyu, Hou Xinglong, Zhang Zaoxiao, Duan Quan. Identification and prediction of fatigue crack growth under different stress ratios using acoustic emission data. Int J Fatigue 2022;160:106860.
[16] Yeasin Bhuiyan Md, Bao Jingjing, Poddar Banibrata, Giurgiutiu Victor. Toward identifying crack-length-related resonances in acoustic emission waveforms for structural health monitoring applications. Struct Health Monit 2018;17(3):577–85.
[17] Karimian Seyed Fouad, Modarres Mohammad, Bruck Hugh A. A new method for detecting fatigue crack initiation in aluminum alloy using acoustic emission waveform information entropy. Eng Fract Mech 2020;223:106771.
[18] Deschanel S, Ben Rhouma W, Weiss J. Acoustic emission multiplets as early warnings of fatigue failure in metallic materials. Sci Rep 2017;7(1):13680.
[19] Deschanel Stéphanie, Weiss Jérôme. Contrôle de la fatigue des matériaux par émission acoustique. 2018, p. 20.
[20] Geller Robert J, Mueller Charles S. Four similar earthquakes in central california. Geophys Res Lett 1980;7(10):821–4.
[21] de la Selle Théotime, Weiss Jérome, Deschanel Stéphanie. Acoustic multiplets detection based on DBSCAN and cross-correlation. Mech Syst Signal Process 2024;211:111149.
[22] Besnard G, Hild François, Roux Stephane. "Finite-element" displacement fields analysis from digital images: Application to Portevin–Le Châtelier bands. Exp Mech 2006;46.
[23] Réthoré J. Ufreckles. 2018, http://dx.doi.org/10.5281/zenodo.1433776.
[24] McNeill SR, Peters WH, Sutton MA. Estimation of stress intensity factor by digital image correlation. Eng Fract Mech 1987;28(1):101–12.
[25] Williams ML. On the stress distribution at the base of a stationary crack. J Appl Mech 1957;24(1):109–14.
[26] Hamam R, Hild F, Roux S. Stress intensity factor gauging by digital image correlation: Application in cyclic fatigue. Strain 2007;43(3):181–92.
[27] Roux Stéphane, Hild François. Stress intensity factor measurements from digital image correlation: post-processing and integrated approaches. Int J Fract 2006;140(1–4):141–57.
[28] Aggelis Dimitrios G, Kordatos Evangelos Z, Matikas Theodore E. Monitoring of metal fatigue damage using acoustic emission and thermography. 11.
[29] Sauerbrunn Christine, Kahirdeh Ali, Yun Huisung, Modarres Mohammad. Damage assessment using information entropy of individual acoustic emissio waveforms during cyclic fatigue loading. Appl Sci 2017;7(6):562.
[30] Pippan R, Hohenwarter A. Fatigue crack closure: a review of the physical phenomena: Fatigue crack closure. Fatigue Fract Eng Mater Struct 2017;40(4):471–95.
[31] Elber Wolf, et al. The significance of fatigue crack closure. 1971.
[32] Schijve J. Four lectures on fatigue crack growth: II. Fatigue cracks, plasticity effects and crack closure. Eng Fract Mech 1979;11(1):182–96.
[33] Schijve J. Shear lips on fatigue fractures in aluminium alloy sheet material. Eng Fract Mech 1981;14(4):789–800.
[34] Bathias Claude, Baïlon Jean-Paul, et al. La fatigue des matériaux et des structures. 1980.
[35] Broek D. Elementary engineering fracture mechanics, vol. 58, Leyden: Noordhoff International Publishing; 1974, 9.
[36] Calvín Giovanna, Escalero Mikel, Zabala Haritz, Muñiz-Calvente Miguel. Distribution of the through-thickness effective stress intensity factor range and its influence on fatigue crack growth rate curves. Theor Appl Fract Mech 2022;119:103374.
[37] Lai MO, Ferguson WG. Relationship between the shear lip size and the fracture toughness. Mater Sci Eng 1980;45(2):183–8.
[38] Dunegan HL, Green AT. Factors affecting acoustic emission response from materials. ASTM International; 1972.
[39] Kohn DH, Ducheyne P, Awerbuch J. Sources of acoustic emission during fatigue of Ti-6Al-4V: effect of microstructure. J Mater Sci 1992;27:1633–41.
[40] Yuyama S, Kishi T, Hisamatsu Y. Effect of environment, mechanical conditions, and materials characteristics on AE behavior during corrosion fatigue processes of an austenitic stainless steel. Nucl Eng Des 1984;81(2):345–55.